Hadronization and Quark Probes of Deconfinement at RHIC

Huan Z. Huang* and Johann Rafelski†

*Department of Physics and Astronomy, University of California, Los Angeles, CA 90095-1547
†Department of Physics, University of Arizona, Tucson, AZ 85721-0081

Abstract. [1] We discuss experimental features of identified particle production from nucleus-nucleus collisions. These features reflect hadronization from a deconfined partonic matter whose particle formation scheme is distinctly different from fragmentation phenomenology in elementary collisions. Multi-parton dynamics, such as quark coalescences or recombinations, appear to be essential to explain the experimental measurements at the intermediate transverse momentum of 2–5 GeV/c. Constituent quarks seem to be the dominant degrees of freedom at hadronization. Heavy quark production should help quantify deconfined matter properties.

Keywords: Quark Gluon Plasma, Deconfinement, Relativistic heavy-ion collisions, Strangeness, Hadronization, Collective Flow, Elliptic Flow, Charm production
PACS: 25.75.Nq,25.75.-q,24.10.Pa,25.75.Dw

1. INTRODUCTION

The advent of the Relativistic Heavy Ion Collider (RHIC) at Brookhaven National Laboratory (BNL) has turned the next page in search for, and study of, the Quark Gluon Plasma (QGP). Most recent dAu baseline reaction measurements by all four RHIC experiments [1, 2, 3, 4] confirmed that a dense strongly interacting medium has been created in central AuAu collisions at RHIC. The QCD nature of the dense matter created at RHIC and whether the current experimental evidence proves the discovery of the QGP have been since under debate within the heavy ion physics community [5, 6, 7, 8]. We will address here primarily the physics 'soft' hadron experimental results and the related evidence for deconfinement. The major topics we address are: 1) features of hadronization and other evidence for a color deconfined bulk partonic matter; 2) the QCD properties of the matter at hadronization; and 3)charm production and related future experimental measurements capable to further quantify the properties of deconfined phase.

Among topics we discuss in depth are: mechanisms of hadronization, experimental status of strange particle production enhancement, azimuthal parton flow anisotropy, bulk properties of dense hadron matter at parton fireball breakup, charm experimental status at RHIC.

[1] This report constitutes the combined contribution of the authors to the "VI Quark Confinement and the Hadron Spectrum" conference, held 21–25 September 2004 in Sardinia, Italy covering their oral presentations and the 'Deconfinement' discussion session; proceedings to be published by the American Institute of Physics.

2. FEATURES OF HADRONIZATION OBSERVED AT RHIC

2.1. What we know about hadronization

We observe, in the final state, a multitude of hadrons, irrespective of what happened and which reaction system is observed. The paradigm emerged that QCD color charges are confined and hadrons exist in color singlet state. Individual reactions occur between leptons and/or quarks. However, the conversion, *i.e.*, hadronization of quarks and gluons (partons) has not been understood based on first principles. There are several widely studied models:

1. Hadron formation in elementary e^+e^- and qq (that is nucleon–nucleon) collisions has been described in the pQCD domain in terms of several components. The particle production process is factorized into parton distribution functions, parton interaction processes and in final step, fragmentation functions for hadron formation.

   The fragmentation function is assumed to be universal and can be obtained phenomenologically from e^+e^- collision measurments. A typical Feynmen-Field [9] fragmentation process involves a leading parton of momentum p, which fragments into a hadron of momentum p_h whose properties are mostly determined by the leading parton. The fragmentation function is a function of variable $z = p_h/p,\ z \in (O,1)$. Note that baryon production is found to be significantly suppressed compared to the production of light mesons: the baryon to pion ratio increases with z, but never exceeds 20% [10], see also the pp-STAR results in figure 2 below.

2. In the soft (low $p_\perp$) particle production region, the pQCD framework and factorization break down, particles are believed not to be from fragmentation of partons. In the elementary interactions physics, string fragmentation models were inspired by the QCD description of the quark and anti-quark interaction. The Lund string model is one of the popular hadron formation models which has been successfully implemented in Monte Carlo description of e^+e^-, pp, and nuclear collisions [11]. Note that, in the string fragmentation models, the baryon production is also suppressed because baryon formation requires the clustering of three quarks [12].

3. Soft multi particle production in particular in the AA (nuclear) collision domain is described within the (Fermi) Statistical Hadronization (SH) model. SH is a model of particle production in which the birth process of each particle fully saturates (maximizes) the quantum mechanical probability amplitude, and thus, all hadron yields are determined by the appropriate integrals of the accessible phase space.

   The statistical hadronization model introduced in 1950 [13, 14] has matured today to a full fledged tool for soft strongly interacting particle production, capable to describe in detail hadron abundances once the mass spectrum of hadron resonances is included [15]. The key SH parameters within the grand canonical formulation of particle phase space are the temperature T and, at a finite baryon density present in a AA reaction system, the baryochemical potential $\mu_{\rm B}$. It is generally accepted

that as the energy of the colliding nuclei varies, a wide domain of T and μ_B is explored, see figure 2 in [16]. Note that the ratio of baryons to mesons is, in chemical equilibrium, also suppressed, since $e^{\frac{m_{\pi,K}-m_{\rm baryon}}{T}} \ll 1$

4. The reaction picture of a soup of quarks in a dense expanding fireball inevitably triggers development of recombination and coalescence models [17, 18]. Recent experimental RHIC results triggered further developments on quark coalescence [19, 20] and recombination [21, 22] which all have the essence of multiparton dynamics for hadron formation, despite significant differences in details.

2.2. (Anti)Baryon yield

Strangeness plays a particularly important role as a characteristic QGP observable. The enhanced production of (strange) (anti)baryons has been an expected feature in recombinant hadronization of QGP. In nuclear collisions, the strange hadron yield derives from two independent reaction steps following each other in time:

1. the establishment of a ready supply of strange quark pairs $s, \bar{s}$ which occurs predominantly in the initial hot phase of bulk partonic matter by the *thermal* pQCD gluon fusion processes $gg \to s\bar{s}$ [23], in a manner independent of the production of final state hadrons;
2. the high initial $s, \bar{s}$ yield survives the process of fireball expansion evolution [17], and contributes in hadronization of pre-formed $s, \bar{s}$ quarks to an unusually high multistrange (anti)baryon abundance [24].

This is illustrated in figure1.

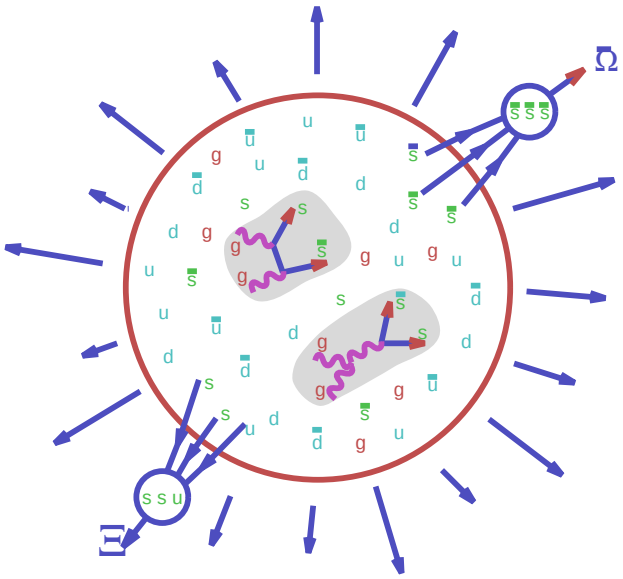

FIGURE 1. Illustration of the two step mechanism of strange hadron formation from QGP: inserts show gluon fusion into strangeness, followed by QGP recombinant hadronization.

Experiments indeed show very significant new features of hadron formation in AA interactions compared to elementary e^+e^- and qq (that is pp) collisions.

- Baryon production from AA collisions, especially for multi-strange hyperons, has been measured to be much larger than theoretical (superposition, cascade) model calculations. The hyperon production per number of participant pairs from AA collisions at the SPS is significantly enhanced in comparison with the value from pp collisions. The enhancement factor increases from Λ to Ω hyperons and with the collision centrality [25, 26].
- The increase in the baryon production from AA collisions has become much more prominent at RHIC energies. Figure 2 shows the ratios of $\overline{p}/\pi$ and $\overline{\Lambda}/K_S$ from central AuAu collisions at $\sqrt{s_{NN}} = 130$, and 200 GeV measured by PHENIX [27] and STAR [28, 29, 30].

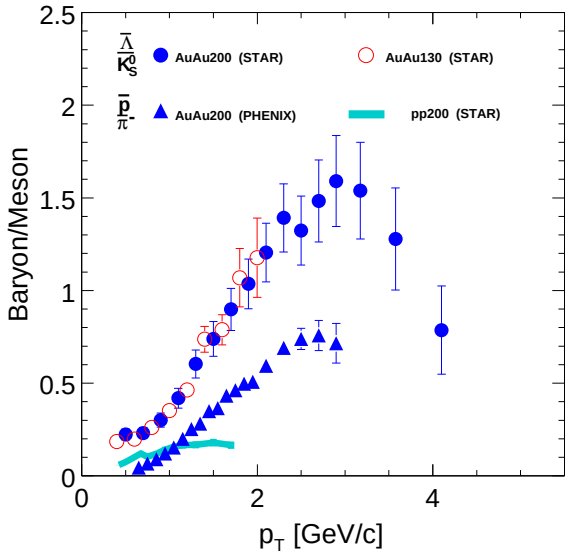

FIGURE 2. Ratios of $\overline{\Lambda}$ to K_S from AuAu and pp collisions (STAR) and $\overline{p}$ to π from AuAu collisions (PHENIX) as a function of transverse momentum ($p_\perp$). In addition to resonance contributions in all hadrons, the $\overline{\Lambda}$ includes contributions from Σ^0 decays.

The apparent difference, in figure 2, between the STAR and PHENIX ratios can be understood since the STAR $\overline{\Lambda}$ data include the electromagnetic decay contribution from Σ^0 and both comprise different 'towers' of hadron resonance decays. Note also that the PHENIX data are corrected for post-reaction weak decay contributions $Y, \overline{Y} \rightarrow N\overline{N}$. Similarly, the STAR $\overline{\Lambda}$ data have been corrected for feed-down contributions from multi-strange hyperon decays. Some early data, for example [31], are not shown because these data were not corrected for weak decay contributions.

The large baryon to meson ratio, seen in figure 2, cannot be accommodated by the traditional, *e.g.*, fragmentation scheme. The large ratio at the intermediate $p_\perp$ region provide clear evidence that particle formation dynamics in AA collisions at RHIC are distinctly different from the traditional hadron formation mechanism via fragmentation processes developed for the elementary e^+e^- and nucleon-nucleon collisions.

The recombination models [21, 22] provided a satisfactory description of the particle yields, in particular, the large production of baryons in the intermediate $p_\perp$ region. The formation of a dense partonic system provides a parton density dependent increase in baryon yield as a function of collision centrality through the coalescence mechanism.

Comparing AuAu with pp reactions at $\sqrt{s_{\rm NN}} = 200\,$GeV, see figure3, we see another large baryon production enhancement for strange (anti)baryons $\Lambda, \overline{\Lambda}, \Xi^-, \overline{\Xi}^+$ reported by STAR [32]. This enhancement increases with centrality [33, 34] and with greater strangeness content as found in strangeness recombination model [17]. These feature were recognized early on as a characteristic signature of QGP [24].

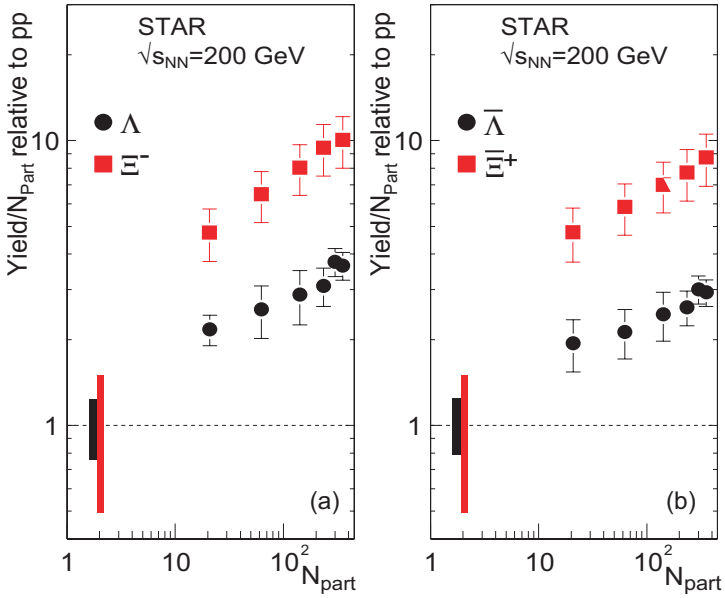

FIGURE 3. The STAR yields per participant for production of Λ and Ξ^- on left (a) and $\overline{\Lambda}$ and $\overline{\Xi}^+$ on right (b) in AuAu collisions at $\sqrt{s_{\rm NN}} = 200\,$GeV. Error bars are statistical. Ranges for pp reference data indicate the systematic uncertainty.

This pattern of baryon enhancement has been observed by the WA97 [25] and NA57 [26] experiments at lower reaction energy available at the CERN-SPS. There is a gradual increase in the strange antibaryon yield with reaction energy [26]. The large difference between baryon and antibaryon yields at SPS energy range are due to the presence of a significant baryon density at lower reaction energy. For purpose of comparison with RHIC results, this baryon density effect can be removed by considering the geometric mean of the baryon and antibaryon yield.

In our opinion, the results presented above for the systematics of strange hadron enhancement demonstrate that same novel mechanism operates in the entire collision energy interval spanned by these data. Only a deconfined quark-gluon plasma is a copious source of these often rarely produced hadrons. When the plasma fireball breaks up into final hadrons, the high abundance of strange quarks and antiquarks manifests itself yielding high abundances of multi strange hadrons. In conventional reaction schemes, the production of particles containing two or more strange quarks is suppressed by the rarity of the required reaction processes.

2.3. Nuclear modification factor

The nuclear modification factor is defined in a collision number scaled comparison of peripheral with central head-on collisions:

$$R_{CP} = \frac{[yield/N_{bin}]^{central}}{[yield/N_{bin}]^{peripheral}}. \quad (1)$$

The nuclear modification factor has also been defined by,

$$R_{AA} = \frac{[yield]^{AA}}{N_{bin} \times [yield]^{pp}}, \quad (2)$$

where N_{bin} is the number of binary nucleon–nucleon collisions. The $[yield]^{AA}$ and $[yield]^{pp}$ are particle yields ($d^2n/dp_\perp dy$) from AA and pp collisions, respectively.

A R_{AA} or R_{CP} of unity implies that particle production from AA collision is equivalent to a superposition of independent nucleon–nucleon collisions. Hard scattering processes within the pQCD framework are believed to follow approximately the binary scaling in the kinematic region where the nuclear shadowing of parton distribution function and the Cronin effect are not significant.

Measurements of charged hadrons and neutral pions have revealed a strong suppression at high $p_\perp$ region in central AuAu collisions [35, 36, 37, 38]. Recent dAu measurements [1, 2, 3, 4] have demonstrated that the large suppression of high $p_\perp$ particles in central AuAu collisions is mainly due to energy loss, presumably of partons traversing the dense matter created in these collisions.

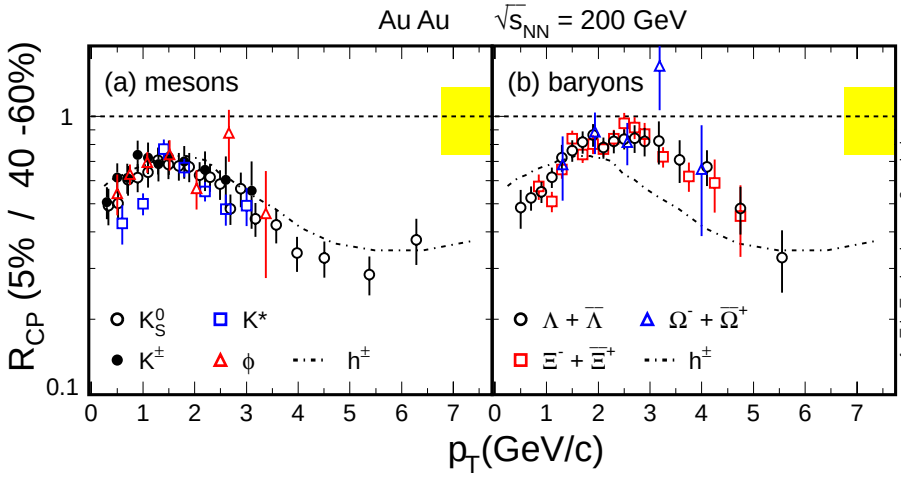

FIGURE 4. R_{CP} of $K^\pm$, K_S, K^*, ϕ, Λ, Ξ and Ω in comparison with charged hadron in dashed line. Distinct meson and baryon groups are observed.

Figure 4 shows the R_{CP} of $K^\pm$, K_S, K^*, ϕ, Λ, Ξ and Ω as a function of $p_\perp$ from AuAu collisions at $\sqrt{s_{NN}} = 200$ GeV measured by the STAR collaboration, where the ratio is derived from the most central 5% to the peripheral $40--60\%$ collisions. The dashed line is the R_{CP} of charged hadrons for reference. In the low $p_\perp$ region, soft particle production is dominated by the number of participant scaling.

The particle type dependence can be described using hydrodynamic flow which predicts a mass dependence for the low $p_\perp$ spectra. In the intermediate $p_\perp$ region of 2 to 5.5 GeV/c the $p_\perp$ dependence of R_{CP} falls into two groups, one for mesons and one for baryons. Despite the large mass differences between K_S and K^*/ϕ, and between Λ and Ξ little difference among the mesons and among the baryons has been observed within statistical errors. Particle dependence in the nuclear modification factor disappears only above a $p_\perp$ of 6 GeV/c, consistent with the expectation from conventional fragmentation processes. The unique meson and baryon dependence in the intermediate $p_\perp$ region indicates the onset of a production dynamics very different from both fragmentation at high $p_\perp$ and hydrodynamic behavior at low $p_\perp$.

2.4. Azimuthal anisotropy

The azimuthal angular particle distribution can be described by a Fourier expansion,

$$\frac{d^2n}{p_\perp dp_\perp d\phi} \propto (1+2\sum_n v_n \cos n(\phi - \Psi_R)), \tag{3}$$

where Ψ_R is the reaction plane angle and v_2 has been called elliptic flow [39]. In a non-central AA collision the overlapping participants form an almond shaped particle emission source, see figure 5. The reaction plane is defined by the vectors x (impact parameter direction) and z (beam direction). The pressure gradient is greater and particles would experience larger expansion force along the short axis direction (in plane) than along the long axis (out plane), see figure 5 left, resulting in the final state in an ellipsoid in transverse momentum space. Theoretical, (typically hydrodynamic) model calculations find that this $p_\perp$ dependent component in v_2 is generated mostly at the early stage of the nuclear collision.

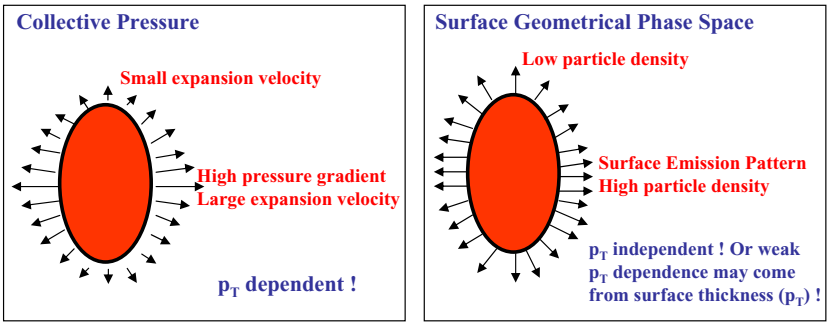

FIGURE 5. Schematic diagram to show two dynamical origins of angular anisotropy, one from hydrodynamical expansion and the other from surface geometrical phase space.

There is another dynamical mechanisms responsible for v_2 due to the spatial geometrical component in the phase space of emitting source. Particle production from a dense matter can be squeezed more in the reaction plane than that out of the reaction plane. More generally, a freeze-out geometry will impose itself on particle abundance ellipticity. However, any $p_\perp$ dependence would be a 2nd order effect associated *e.g.* with the

optical depth of the freeze-out system. Figure 5 shows a schematic diagram for these two mechanisms of generating azimuthal angular anisotropy v_2 in non-central collisions.

Figure 6 shows the v_2 as a function of $p_\perp$ for π, K, p, Λ and Ξ from PHENIX [40] and STAR [41] measurements. The angular anisotropy v_2 reveals three salient features:

1. particles exhibit hydrodynamic behavior in the low $p_\perp$ region — a common expansion velocity may be established from the pressure of the system and the heavier the particle the larger the momentum from the hydrodynamic motion leading to a decreasing ordering of v_2 from π, to K and p for a given $p_\perp$;
2. v_2 values do not depend strongly on $p_\perp$ at the intermediate $p_\perp$ region in contrast to the strong $p_\perp$ dependence in the yield of particles;
3. the saturated v_2 values for baryons are higher than those for mesons and there is a distinct grouping among mesons and baryons.

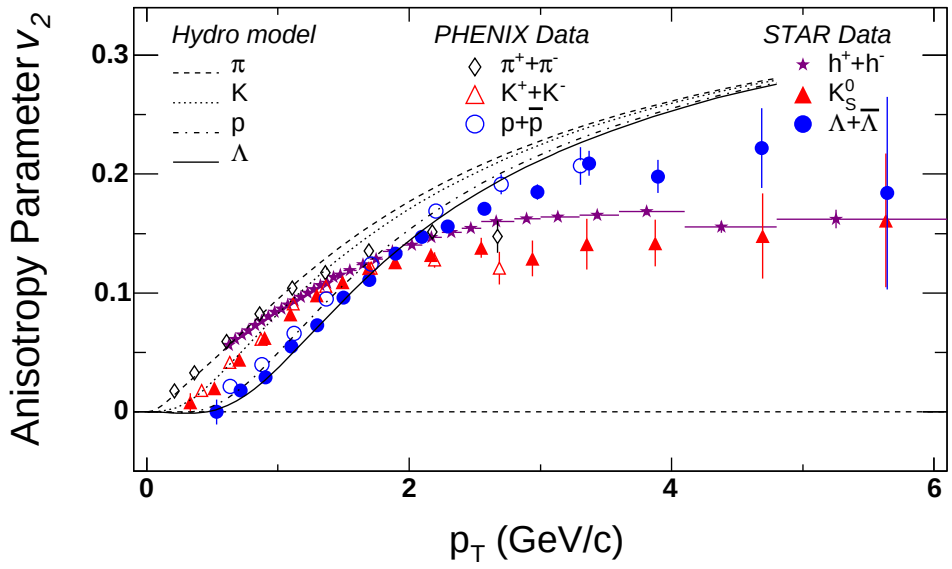

FIGURE 6. Azimuthal angular anisotropy v_2 as a function of $p_\perp$ for identified particles. The hydrodynamic calculation results are by P. Huovinen *et al.* [42].

The absence of a strong $p_\perp$ dependence at the intermediate $p_\perp$ region is an intriguing phenomenon for the angular anisotropy of particle emission. Parton energy loss in the dense medium created in AA collisions was proposed as a possible mechanism for generating an angular anisotropy v_2. High energy partons are quenched inside the dense medium and lead to an effective particle emission just from a shell area of the participating volume [43]. Jet quenching scenario [44] (parton energy loss scenario) cannot explain the particle dependence in both the nuclear modification factor and the angular anisotropy v_2 at the intermediate $p_\perp$ region. Within the parton energy loss scenario the larger v_2 of baryons implies a higher energy loss than that of mesons; the larger nuclear modification factor of baryons, however, is only consistent with a smaller energy loss than that of mesons. This scenario may be important for the considerable v_2 magnitude for charged hadrons at a $p_\perp$ greater than 6 GeV/c or so measured by STAR [45].

Indeed, the magnitude of the measured v_2 is significantly larger than what can be accommodated based on particle emission from a geometrical ellipsoid source within an energy loss scenario [46]. Using a more realistic Wood–Saxon description of the colliding nuclei for the ellipsoid source, the predicted theoretical v_2 is much smaller than that from a hard-sphere model of the colliding nuclei, leading to a greater discrepancy between the measurement and the theoretical expectation.

We conclude that the magnitude and the particle dependence of v_2 at the intermediate $p_\perp$ region cannot have a dynamical origin either from hydrodynamic flow or from parton energy loss alone. Another plausible procedure would be to relate the v_2 in the intermediate $p_\perp$ region to the geometrical shape of the emitting particle source, see figure 5. A surface emission pattern from the almond shaped participant volume should naturally lead to a saturation of v_2. A surface emission scenario is possible if particles are produced by surface related dynamical instabilities and the hadronization duration is relatively short [47].

2.5. Quark Flow Anisotropy

An empirical quark number n scaling of v_2 has been noted [48]. n is the number of valance quarks and antiquarks in a hadron. Figure 7 presents the v_2/n as a function of $p_\perp/n$ for K, p, Λ and Ξ from AuAu200 collisions, where the line is a polynomial fit to the data points. The bottom panel shows the ratio of data points to the fit. At the intermediate $p_\perp$ region ($0.6 < p_\perp/n < 2$ GeV/c), all meson and baryon data points fall onto an uniform curve. The π data (not shown) are significantly above the v_2 of other mesons. The large fraction of resonance decay contribution to the π yield is known to enhance the v_2 of π at a given $p_\perp$ [49, 50].

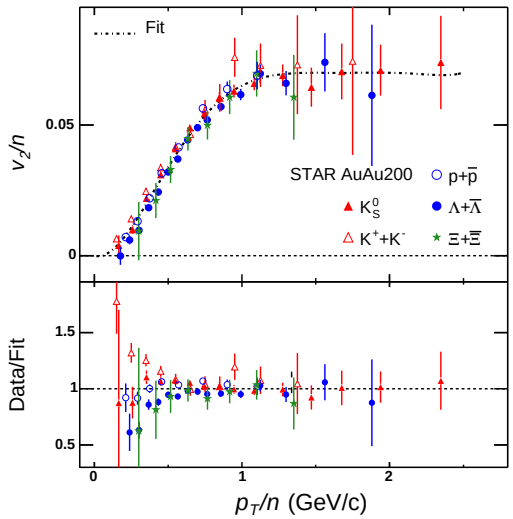

FIGURE 7. Azimuthal angular anisotropy v_2/n as a function of $p_\perp/n$ for identified particles where n is the number of constituent quarks. The line is a polynomial fit to the data points excluding the π data. The bottom panel shows the (multiplicative) deviation from the fit line.

For $p_\perp/n < 0.6$ GeV, there appears a small residual but systematic particle dependent deviation from the fit curve, which agrees best with the K_S results. The residual mass and/or strangeness and/or meson–baryon dependence of this deviation can have many causes involving microscopic transport and/or collective flow phenomena. Its detailed understanding could play an important role in the demonstration of physics processes that lead to the constituent quark level azimuthal flow at hadronization.

We believe that the particle dependence on v_2, which is largley explained by n-scaling, requires a v_2 distribution at the constituent quark level. The scaled azimuthal angular anisotropy (v_2/n) may be interpreted as the constituent quark anisotropy just prior to the hadron formation. The n-scaling works both for strange and nonstrange quarks, indicating that the azimuthal flow anisotropy is the same for all three 'light' flavors, and by extension, that the collective quark flow is the same for the three flavors. The precision of the n scaling leaves very little space for the presence of gluon (fragmentation) participation in the intermediate momentum particle production process. This suggests that semi-hard gluons have effectively disapperad as independent partonic degrees of freedom in the final hadron formation.

We have shown in this section that the hadron formation dynamics, at RHIC at $0.6 < p_\perp/n < 2$, GeV/c is very different from the parton fragmentation picture where the leading parton plays a dominant role in determining properties of the final state hadron. The measured features for these intermediate $p_\perp$ hadrons produced at RHIC require that all quark ingredients ($n = 2$ for mesons and $n = 3$ for baryons) play an approximately equal role in the hadron formation and that the hadron properties are determined by the sum of contributing partons.

3. DECONFINED BULK MATTER

3.1. Bulk properties as function of centrality

The global study of soft hadron yields and spectra implies that we can fully characterize the properties of bulk matter at time of hadronization by adding up strangeness, entropy, etc., contained in the final state hadrons [51]. This is done particularly easily within the statistical hadronization scheme, which have been successfully applied to describe stable particle production.

As a first step, this leads to a quantitative understanding of the variation of the bulk properties with centrality [52]. In such an analysis of $\sqrt{s_{NN}} = 200$ GeV STAR and PHENIX results, the contents in entropy, baryon number, strangeness, and energy grows linearly with the participant number for $A > 20$. This implies that the conversion of colliding nuclear matter into bulk parton matter is at RHIC rather independent of the size of nuclear overlap and complete, including all matter. In our above discussion of v_2, we have tacitly assumed that the properties of bulk partonic matter formed in non central collisions are not significantly dependent on centrality, as the present study confirms

In most central 5% of the reactions, one finds that the net baryon density per unit of rapidity is at mid-rapidity $d(B-\overline{B})/dy = 14 \pm 2$, the strangeness yield $ds/dy = 135 \pm 10$ and the entropy yield $dS/dy = 4900 \pm 400$. The errors comprise the uncertainty of the data and the chemical scheme used. The strangeness per entropy yield $s/S = (2.9 \pm$

$0.3)10^{-3}$ is more than 4 times enhanced compared to the AGS energy scale. For the most peripheral reactions, this ratio is $s/S = (1.9 \pm 0.3)10^{-3}$ which shows the influence of the fireball expansion dynamics on production of strangeness.

Given the experimental yields of particles at central rapidity, the intensive properties of bulk matter at hadronization, such as P pressure, ε energy density, σ entropy density, $E/TS = \varepsilon/T\sigma$, seen in figure 8, follow summing the properties of individual particle fractions. They are given for the two chemical models in figure 8 on left. The lines guide the eye, the actual results are the squares and circles centered at the mean trigger centrality of the data considered. These results are for the full chemical non-equilibrium (squares) and for strangeness chemical non-equilibrium (circles) respectively.

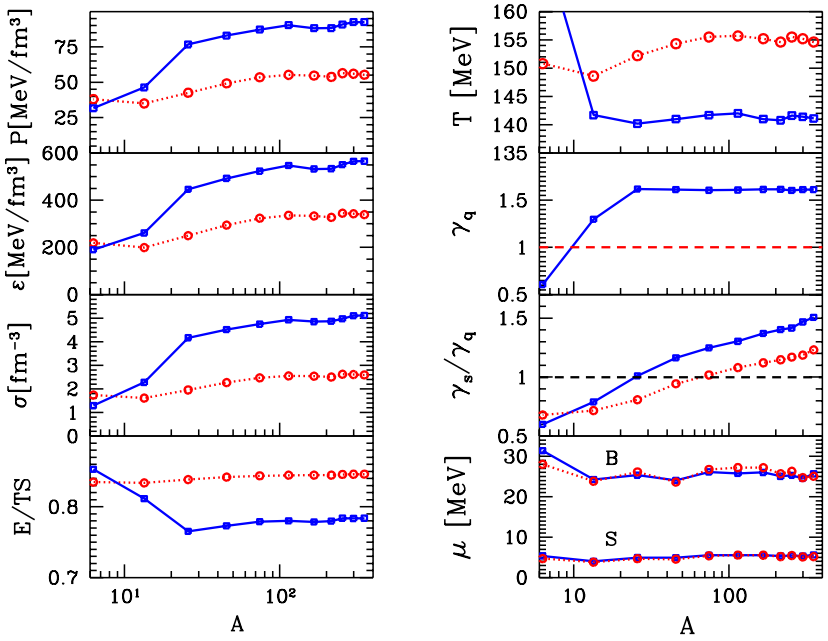

FIGURE 8. Left: pressure P, energy density $\varepsilon = E/V$, entropy density S/V and E/TS and; Right: temperature T, light quark phase space occupancy γ_q, the ratio of strange to light quark phase space occupancies γ_s/γ_q and the chemical potentials (B for baryochemical μ_B and S for strangeness μ_S) as a function of centrality. After Ref. [52].

To obtain the physical properties, a fit of the statistical hadronization model parameters had been performed and the results are shown on right: the hadronization temperature T, phase space occupancies $\gamma_q, \gamma_s/\gamma_q$, and the chemical potential $\mu_{B,S}$ of baryon number and strangeness, respectively. We see the expected rise of strangeness occupancy yield with size (centrality) of the system, related to the extended lifespan during which strangeness is produced [33, 34]. Otherwise there is remarkable stability of the bulk properties with centrality of the collision. The bulk matter created at RHIC at $\sqrt{s_{\rm NN}} = 200$ GeV, small or large in size and independently of models of chemical (non)equilibrium has a baryochemical potential $\mu_{\rm B} = 25 \pm 1$ MeV.

3.2. The Phase Boundary

The hadronization temperature $T = 140$–155 ± 8 MeV is near but below the phase transformation boundary for QCD with 2+1 flavors. The infinite matter static equilibrium transformation is expected at $T = 164 \pm 4$ MeV, for more detail about the structure of the cross-over region, see figure 9.

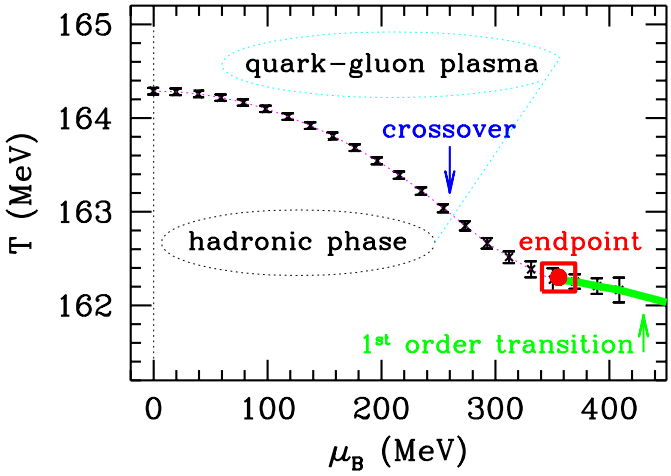

FIGURE 9. The phase diagram at low baryon density in physical units, results of Ref. [53]. Phase crossover ends in the square which shows the endpoint where 1st order phase transition sets in.

The lower RHIC freeze-out temperature we reported above is associated with a rapid expansion of the RHIC fireball: the flow of color charge pushes the vacuum and the bulk breakup occurs suddenly from an over expanded supercooled condition. Quantitatively the supercooling is of the required magnitude [47]. The sudden hadronization mechanism also explains why single freeze-out analysis of particle spectra at SPS and RHIC succeed [54, 55].

4. HEAVY QUARKS

4.1. Theoretical remarks

Heavy quarks (charm, in future bottom) are produced mostly in initial parton scattering (gluon fusion) and in any case during the initial primary and/or very high temperature phase of the collision. Therefore, heavy quark measurement can probe the initial parton flux, the dynamical evolution and the quark energy loss in dense medium. If heavy quarks are found to participate in the collective motion of the medium (radial or elliptic flow), this will lend further confirmation for parton collectivity.

At RHIC, one expects that multiple heavy quark–antiquark pairs will be produced in an individual *AA* collision. Therefore one can expect a novel mechanism of J/Ψ formation by recombination [56]. Then, there should be a contribution to heavy quarkonium formation which utilizes combinations of initially uncorrelated quark and antiquark, leading to a *quadratic* increase with the total number of heavy flavor quarks in

the event. This can occur within the deconfined phase, considering that recent Lattice QCD (LQCD) calculations indicate that spectral functions of pseudo scalar and vector mesons have non-trivial shapes at a temperature above the critical T_c [57]. In particular, heavy quarkonium such as J/ψ may survive at a temperature above $1.6T_c$ [58, 59].

Charm quark transport dynamics in dense nuclear medium will provide unique probes to the QCD properties of the medium. If the initial temperature is very high, $T \sim 500$ MeV or higher, the yield of total charm quarks can also be increased through thermal gluon–gluon scatterings. Possible suppression of charm mesons at high $p_\perp$ will test the energy loss dynamics of charm quark propagation in a QCD medium. Theoretical calculations have predicted a reduced medium induced energy loss for heavy quarks and the high $p_\perp$ suppression of charmed hadrons should not be as strong as light hadrons [60, 61]. For a recent review of theoretical charm quark situation see Ref. [62].

4.2. RHIC experimental status

Both the STAR and PHENIX collaborations at RHIC have been pursuing vigorous heavy quark physics programs, both in analysis of current data and in future detector upgrade plans, to provide better capabilities for heavy quark measurements.

The total charm quark pair production cross section ($\sigma_{c\bar{c}}$) is an important constraint on the collision dynamics and the heavy quark evolution. Both STAR and PHENIX have presented results on the $\sigma_{c\bar{c}}$ measurement of pp collisions from charm semi-leptonic decays. In addition, STAR has also derived an equivalent $\sigma_{c\bar{c}}$ for pp collisions based on direct reconstruction of hadronic decays of charm mesons from dAu collisions. Figure 10 shows the $p_\perp$-spectra of electron and D^0 from STAR. The PHENIX preliminary non-photonic electron data are represented by the fitted line with a reported measurement $\sigma_{c\bar{c}} = 709 \pm 85(\text{stat}) + 332 - 281(\text{sys})\ \mu b$ [63]. STAR has measured $\sigma_{c\bar{c}} = 1300 \pm 200 \pm 400\ \mu b$ and a mean transverse momentum for D^0 of $\langle p_\perp \rangle = 1.32 \pm 0.08$ GeV/c from direct D^0 reconstruction [64]. A next-to-leading order pQCD calculation of the charm quark production cross section [65] has yielded $\sigma_{c\bar{c}} = 300$ — $450\ \mu b$, significantly below the STAR measurement and at the lower end of the PHENIX range of uncertainty.

Several comments on the cross section measurements are in order. When measuring the charm cross section through semi-leptonic decay, the quality of the electron data for $p_\perp \lesssim 1$ GeV/c is significantly deteriorated because of a large combinatorial background. An electron of $p_\perp \sim 1$ GeV/c typically comes from the decay of a D meson with $p_\perp \sim 2$ GeV/c, which is significantly beyond the average $p_\perp$ of 1.32 ± 0.08 GeV/c reported by STAR. Therefore, one has to extrapolate to the low $p_\perp$ region by over a factor of two to obtain the total charm cross section. Such an extrapolation is often model dependent and has a large uncertainty. The semi-leptonic decay branching ratios for D^0, D^*, $D^\pm$ and D_S are different. The electron yield from decays of these D mesons depends on the relative yield which is another important contribution to the uncertainties of the charm production cross section derived from electron measurement. The direct reconstruction of the D decay kinematics provides a broad coverage of $p_\perp$ and does not suffer from the same uncertainties as the leptonic decay electron measurement. However, present

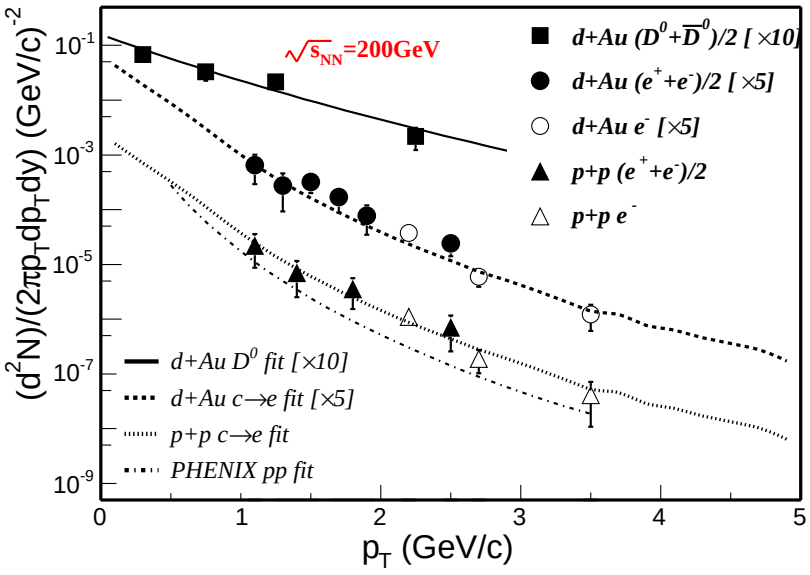

FIGURE 10. $p_\perp$ distribution of D^0 mesons and non-photonic electrons from semi-leptonic decays of charm mesons.

STAR measurements of D meson yields using event-mixing methods from TPC tracks suffer from limited statistics. A future vertex detector upgrade capable of measuring the D decay vertex displacement is essential for both STAR and PHENIX heavy flavor physics programs.

Figure 11 presents the STAR preliminary transverse momentum spectrum of D mesons from dAu collisions normalized by the number of binary collisions, where the $p_\perp$ shapes of D^* and $D^\pm$ are assumed to be the same as that of D^0 [66]. The shape of the $p_\perp$ distribution coincides with the bare charm quark $p_\perp$ distribution from the Fixed-Order-Next-Leading-Log (FONLL) pQCD calculation from M. Cacciari *et al.* [67]. If a fragmentation function such as the Lund fragmentation scheme [68] or the Peterson function [69] is introduced for D meson production, the resulting $p_\perp$ distribution will be significantly below the measurement at the high $p_\perp$ region. This observation raises an outstanding question regarding the $p_\perp$ distribution and the formation mechanism of D mesons in hadro-production. Recently, a $k_\perp$ factorization scheme has been found to significantly change the D meson p_T distribution from nuclear collisions as well [70].

The fact that the D meson $p_\perp$ distribution can be better described by the $p_\perp$ of bare charm quarks from pQCD calculations has been observed in previous fixed target experiments [71]. With a fragmentation function such as the Peterson function the D meson $p_\perp$ distribution is too steep to explain the measured $p_\perp$ distribution. In order to match the calculation with the data one has to introduce a $k_\perp$ kick to the parton distribution. The scale of $\langle k_\perp^2 \rangle$ is on the order of 1 (GeV/c)^2, much larger than the typical Λ_{QCD} scale for strong interaction. Furthermore, the Feynman x_F of the D meson distribution was also found to coincide with the bare charm quark x_F distribution [71]. The fragmentation function will have a large impact on the x_F distribution from bare charm quark to D meson, which cannot be negated by introducing any k_L longitudinal boost of reasonable

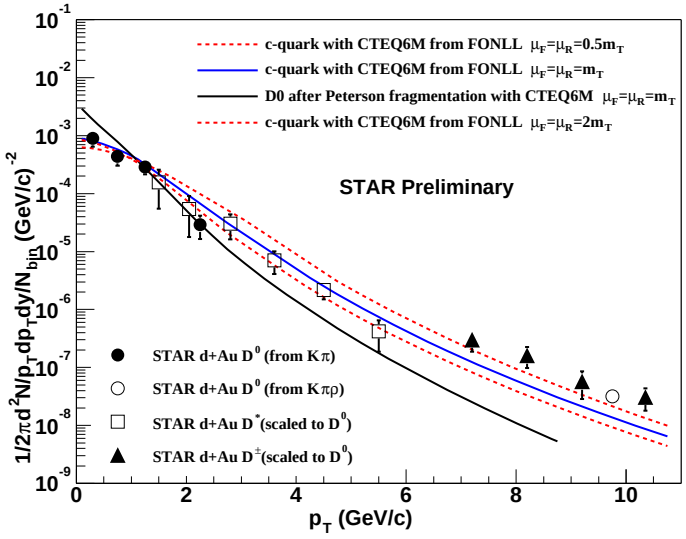

FIGURE 11. STAR preliminary measurement of $p_\perp$ distribution of D mesons from dAu collisions normalized by the number of binary collisions. The shape of the $p_\perp$ distribution is compared to pQCD FONLL calculations.

scale as in the case for $k_\perp$ kick in the transverse momentum direction.

The transverse momentum distribution of particles produced at RHIC energies are considerably flatter than those at lower energies. The $k_\perp$ kick scheme does not change the shape of the $p_\perp$ distribution significantly. The STAR measurement of the D meson $p_\perp$ distribution suggests either that the charm quark fragmentation may be close to a delta function or that a charm formation mechanism such as the recombination model may be important in hadro-production. The recombination model takes a charm quark and combines it with a light quark, presumably of low $p_\perp$, to form a charmed meson. Therefore, the $p_\perp$ of the meson is not significantly different from that of the bare charm quark. In that way, measurements of charmed meson production provide unique probes for the hadron formation dynamics and for the transport dynamics of heavy quarks in the dense nuclear medium produced at RHIC energies.

Observation of heavy quark hydrodynamic flow would indicate that heavy quarks, once created in the initial state, must have participated in the partonic hydrodynamic evolution over a sufficiently long period of time to reach a substantial flow magnitude. This would be a unique probe for the early stage of a partonic phase [72]. Figure 12 shows preliminary STAR [73] and PHENIX [74] measurements of the v_2 for electrons from charm leptonic decays, which have been demonstrated to be closely correlated with charmed meson v_2 [50].

5. SUMMARY

Among the most important aspect of many results presented is that the gluon degrees of freedom are not explicitly manifested in the hadron formation. Quarks are the dominant

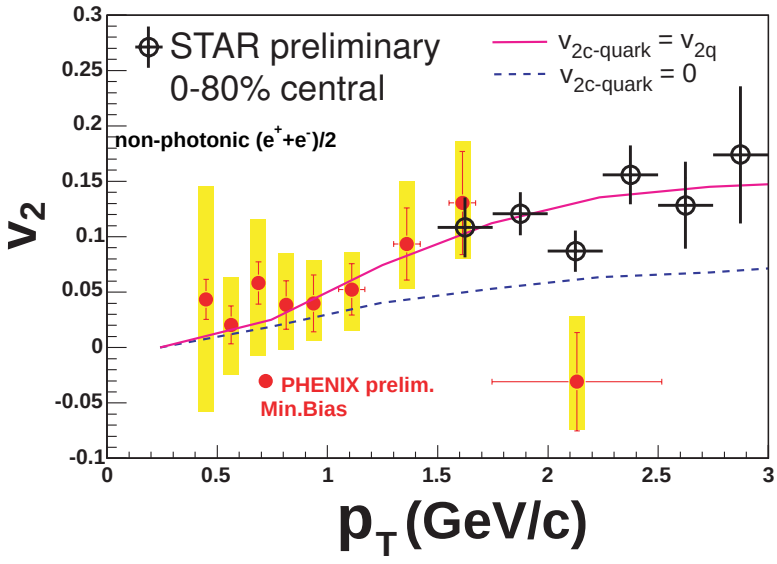

FIGURE 12. Preliminary measurement of non-photonic electron v_2 as a function of p_T from PHENIX and STAR. The curves are from a calculation by V. Greco *et al.* [72].

degrees of freedom at the boundary of quark–hadron transition. It is a critical step to firmly connect this mainly experimental insights on the properties of the quark matter at the boundary of hadronization with the LQCD calculations. The disappearance of the gluon degrees of freedom from the initial state and the emergence of constituent quarks at hadronization are some of the critical conceptual questions to be addressed in the imminent future [75].

Strange (anti) baryon production enhancement at RHIC as function of centrality, energy and $p_\perp$ is significant. For $p_\perp \lesssim 5$ GeV/c, relative baryon to meson yields have shown distinct features that are drastically different from the fragmentation processes in elementary collisions. A novel feature of meson and baryon dependence has been observed in the nuclear modification factor and the angular anisotropy v_2 of π, $K^{\pm}$, K_S, K^*, p, Λ and Ξ particles at the intermediate $p_\perp$ of 2–5 GeV/c. A constituent quark number scaling has been observed for the v_2 measurement. These experimental measurements suggest that quarks have developed a collective v_2 as a function of $p_\perp$; and the hadron formation at the intermediate $p_\perp$ is likely through multi-parton dynamics such as recombination or coalescence process.

This physical picture emerging from the experimental measurements complements the Lattice QCD results. Spectral function calculations have indicated that hadrons, particularly heavy quarkonium, do not melt completely at critical temperature. It appears plausible that the constituent quark degrees of freedom or even hadron-like quasi-particles play a dominant role at the hadronization of bulk partonic matter though further confirmation of the picture from LQCD is needed. We note the related theoretical models [76], which invoke the notion of quasi-hadrons to describe properties of the dense matter.

We have also described how heavy (charm) quark production and its transport dynamics in dense nuclear medium probe QCD properties of the matter. The charm quark flow measurement will provide a significant insight on recombination or coalescence hadronization mechanism and partonic collectivity of the dense matter. Charmonium enhancement arises from a dense charm rich state. Future detector upgrades from STAR and PHENIX will greatly enhance their heavy quark measurement capabilities at RHIC.

Despite intriguing experimental observations of hadronization from a deconfined bulk partonic matter, a smoking colt signatures for the quark–hadron phase transition remain elusive. On the other hand, the totality of experimental results can be understood invoking deconfinement.

ACKNOWLEDGMENTS

We thank An Tai, Hui Long, Paul Sorensen, Xin Dong, Frank Laue, Zhangbu Xu, Nu Xu, Charles Whitten Jr., Jean Letessier, Giorgio Torrieri, Robert Thews for many stimulating discussions on physics topics in this article. We thank Nora Brambilla, Giovanni Prosperi, and the local organizers of the "VI Quark Confinement and the Hadron Spectrum" conference, for their very kind hospitality in Sardinia.

REFERENCES

1. J. Adams *et al.*, Phys. Rev. Lett. **91**, 072304 (2003).
2. S. S. Adler *et al.*, Phys. Rev. Lett. **91**, 027303 (2003).
3. B.B. Back *et al.*, Phys. Rev. Lett. **91**, 027302 (2003).
4. I. Arsene *et al.*, Phys. Rev. Lett. **91**, 027305 (2003).
5. M. Gyulassy and L. McLerran, Preprint nucl-th/0405013 (2004).
6. K. Adcox *et al.*, Preprint nucl-ex/0410003 (2004).
7. J. Adams *et al.*, Preprint nucl-ex/0501009 (2005).
8. B. Muller, Preprint nucl-th/0404015 (2004).
9. R. D. Field and R. P. Feynman, Nucl. Phys. B**136**, 1 (1978).
10. K. Abe *et al.*, Phys. Rev. D**69**, 072003 (2004).
11. Bo Andersson, 'The Lund Model' Cambridge Monogr. Part. Phys. Nucl. Phys. Cosmol. 7 (1997).
12. Bo Andersson *et al.*, Phys. Scripta **32**, 574 (1985).
13. E. Fermi, Prog. Theor. Phys. **5**, 570 (1950).
14. I. Pomeranchuk, Proc. USSR Academy of Sciences (in Russian) **43**, 889 (1951). Translated in: "Quark–Gluon Plasma: Theoretical Foundations" An annotated reprint collection; Edited by J. Kapusta, B. Muller and J. Rafelski ISBN: 0-444-51110-5 , 836 pages , Elsevier, New York, (2003).
15. R. Hagedorn, Suppl. Nuovo Cimento **2**, 147 (1965).
16. R. Hagedorn and J. Rafelski, Phys. Lett. B **97**, 136 (1980).
17. P. Koch, B. Muller and J. Rafelski, Phys. Rept. **142**, 167 (1986).
18. J. Rafelski and M. Danos, Phys. Lett. B **192**, 432 (1987).
19. D. Molnar and S. A. Voloshin, Phys. Rev. Lett. **91**, 092301 (2003).
20. Z. W. Lin and C. M. Ko, Phys. Rev. Lett. **89**, 202302 (2002).
21. R. J. Fries *et al.*, Phys. Rev. Lett. **90**, 202303 (2003).
22. R. C. Hwa and C. B. Yang, Phys. Rev. C**67**, 034902 (2003).
23. J. Rafelski and B. Muller, Phys. Rev. Lett. **48**, 1066 (1982) [Erratum-ibid. **56**, 2334 (1986)].
24. J. Rafelski, Phys. Rept. **88**, 331 (1982).
25. E. Andersen *et al.* [WA97 Collaboration],Phys. Lett. B **449**, 401 (1999).
26. D. Elia [NA57 Collaboration], Preprint nucl-ex/0410034 (2004).
27. S. S. Adler *et al.*, Phys. Rev. C**69**, 034909 (2004).

28. C. Adler *et al.*, Phys. Rev. Lett. **89**, 092301 (2002).
29. J. Adams *et al.*, Phys. Rev. Lett. **92**, 112301 (2004).
30. J. Adams *et al.*, Phys. Lett. B**595**, 143 (2004).
31. K. Adcox *et al.*, Phys. Rev. Lett. **88**, 242301 (2002).
32. H. Caines, Preprint nucl-ex/0412015 (2004).
33. J. Rafelski and J. Letessier, Phys. Lett. B **469**, 12 (1999).
34. J. Letessier, A. Tounsi and J. Rafelski, Phys. Lett. B **389**, 586 (1996).
35. C. Adler *et al.*, Phys. Rev. Lett. **89**, 202301 (2002).
36. J. Adams *et al.*, Phys. Rev. Lett. bf 91, 172302 (2003)
37. K. Adcox *et al.*, Phys. Rev. Lett. **88**, 022301 (2002)
38. S. S. Adler *et al.*, Phys. Rev. Lett. **91**, 072301 (2003).
39. H. Sorge, Phys. Rev. Lett. **82**, 2048 (1999).
40. S. S. Adler *et al.*, Phys. Rev. Lett. **91**, 182301 (2003).
41. J. Adams *et al.*, Phys. Rev. Lett. **92** 052302 (2003).
42. P. Huovinen *et al.*, Phys. Lett. B**503**, 58 (2001).
43. B. Muller, Phys. Rev. C**67**, 06190 (2003).
44. M. Gyulassy *et al.*, Phys. Lett. B**526**, 301 (2002).
45. J. Adams *et al.*, Preprint nucl-ex/0409033 (2004).
46. E. V. Shuryak, Phys. Rev. C**66**, 027902 (2002).
47. J. Rafelski and J. Letessier, Phys. Rev. Lett. **85**, 4695 (2000).
48. P. R. Sorensen, Ph.D. Thesis UCLA, nucl-ex/0309003 (2003).
49. V. Greco and C. M. Ko, Phys. Rev. C**70**, 024901 (2004).
50. X. Dong *et al.*, Phys. Lett. B**597**, 328 (2004).
51. J. Rafelski and J. Letessier, Acta Phys. Polon. B **34**, 5791 (2003).
52. J. Rafelski, J. Letessier and G. Torrieri, Preprint nucl-th/0412072 (2004).
53. Z. Fodor and S. D. Katz, JHEP **0404**, 050 (2004).
54. G. Torrieri and J. Rafelski, New J. Phys. **3**, 12 (2001).
55. W. Broniowski and W. Florkowski, Phys. Rev. Lett. **87**, 272302 (2001).
56. R. L. Thews, M. Schroedter and J. Rafelski, Phys. Rev. C **63**, 054905 (2001).
57. P. Petreczky, J. Phys. G:Nucl. Part. Phys. **30**, S431 (2004).
58. M. Asakawa and T. Hatsuda, Phys. Rev. Lett. **92**, 012001 (2004).
59. F. Karsch, J. Phys. G**30**, S887 (2004).
60. Y. L. Dokshitzer and D. E. Kharzeev Phys. Lett. B**519**, 199 (2001).
61. M. Djordjevic and M. Gyulassy, Phys Lett B**560**, 37 (2003).
62. R. L. Thews, Preprint hep-ph/0412323 (2004).
63. S. Kelly (The PHENIX Collaboration), J. Phys. G**30**, S1189 (2004).
64. J. Adams *et al.*, Preprint nucl-ex/0407006 (2004).
65. R. Vogt, Preprint hep-ph/0203151 (2002).
66. A. Tai (The STAR Collaboration), J. Phys. G**30**, S809 (2004).
67. M. Cacciari, S. Frixione and P. Nason, JHEP **0103**, 006 (2001).
68. T. Sjostrand *et al.*, PYTHIA 6.3: Physica and Manual hep-ph/0308153 (2003).
69. C. Peterson *et al.*, Phys. Rev. D**27**, 105 (1983).
70. D. Kharzeev and K. Tuchin, Nucl. Phys. A**735**, 248 (2004).
71. S. Frixione *et al.*, Adv. Ser. Direct. High Energy Phys. 15 (1998); Preprint hep-ph/9702287 (1997).
72. V. Greco, C. M. Ko and R. Rapp, Phys. Lett. B**595**, 202 (2004).
73. F. Laue (The STAR Collaboration), Preprint nucl-ex/0411007 (2004).
74. M. Kaneta (The PHENIX Collaboration), J. Phys. G**30**, S1217 (2004).
75. A. Maas, J. Wambach, B. Gruter and R. Alkofer, Preprint hep-ph/0411289 (2004), in this volume.
76. G. E. Brown *et al.*, Preprint nucl-th/0402207 (2004).